Published in final edited form as:
Biochemistry. 2013 July 23; 52(29): . doi:10.1021/bi400320s.

Thermodynamic and Structural Analysis of Human NFU Conformational Chemistry

Jingwei Li[1], **Shu Ding**[1], and **J. A. Cowan**[1,2,*]

[1]Evans Laboratory of Chemistry, Ohio State University, 100 West 18th Avenue, Columbus, Ohio 43210

[2]The Ohio State Biochemistry Program, 784 Biological Sciences 484 W. 12th Avenue, Columbus, Ohio 43210

Abstract

Human NFU has been implicated in the formation of inorganic sulfide required for cellular iron-sulfur cluster biosyntheses. The protein contains a well-structured N-terminal domain and a C-terminal domain with molten globule characteristics that also contains a thioredoxin-like pair of redox active Cys that promote persulfide reductase activity. Recent reports have highlighted the existence of structural flexibility in the ISU/IscU-type scaffold proteins that mediate Fe-S cluster assembly, which is also likely to serve an important role in the pathway to iron-sulfur cluster maturation. We have previously reported similar structural mobility for the C-terminal domain of human NFU, a protein that has been implicated in the production of sulfide for cluster synthesis, while homologous proteins have also been suggested to serve as Fe-S cluster carriers. Herein we quantitatively characterize the structural stability of the two domains of human NFU, and in particular the functional C-terminal domain. The results of differential scanning calorimetry (DSC) and variable temperature circular dichroism (VTCD) studies that have been used to analyze the temperature-dependent structural melting profiles of the N- and C-terminal domains, relative to both full-length NFU and an equimolar ratio of the N- and C-terminal domains, and correlated with structural information derived from NMR. Calorimetry results indicate that the C-terminal NFU domain undergoes a significant structural stabilization following interaction with the N-terminal domain, which resulted in a novel and distinctive transition melting profile (T_m^{sec} = 58.1 ± 0.4 °C, ΔH_v^{sec} = 60.4 ± 5.3 kcal/mol, T_m^{ter} = 49.3 ± 0.3 °C, ΔH_v^{ter} = 71.8 ± 5.8 kcal/mol). VTCD experiments also revealed a secondary structure transition at 59.2 °C in agreement with calorimetry results. The degree of stabilization was found to be more significant in the full-length NFU, as the C-terminal domain transitions were recorded at higher temperatures (T_m^{sec} = 63.3 ± 3.4 °C, ΔH_v^{sec} = 41.8 ± 8.2 kcal/mol). The interactions between the two domains demonstrated the hallmarks of hydrophobic character, as increased ionic strength decreased the degree of stabilization of the C-terminal domain. An increase of 2% in α -helix content further supports interaction between the two domains leading to greater secondary structure stabilization. Heteronuclear single quantum coherence (HSQC) experiments indicate the C-terminal domain to adopt an alternate tertiary conformation following binding to the N-terminal domain. The structural rigidity of the N-terminal domain leads to an alternative conformation for the C-terminal domain, suggesting that such an interaction, although weaker compared to the covalently-attached native NFU, is important for the structural chemistry of the native full-length protein. The results

Correspondence to: Dr. J. A. Cowan, Evans Laboratory of Chemistry, Ohio State University, 100 West 18th Avenue, Columbus, Ohio 43210. tel: 614-292-2703, cowan@chemistry.ohio-state.edu.

The authors declare no competing financial interest.

Supporting Information Available.

Electronic Supplementary Information (ESI) available: details of protein expression, purification, CD, DSC and NMR experiments. This material is available free of charge via the Internet at http://pubs.acs.org (DOI: 10.1039/b000000x/)

also emphasize the likely general importance of such structural flexibility in select proteins mediating metal cofactor biosynthesis.

Keywords

NFU; VTCD; DSC; NMR; molten globule

Introduction

Human NFU is a multifunctional protein that has been demonstrated to interact with the histone cell cycle regulation homologue A (HIRA) as a transcriptional regulator due to its ability to influence the chromatin structure.[1,2] Human NFU has also been linked to Lafora disease due to its interaction with laforin, a protein which is found to be mutated in the disease state.[3] NFU family proteins have also been implicated in cellular iron-sulfur cluster biosyntheses, both *in vivo* and *in vitro*.[4-11] For example, the functional site[11] of human NFU is located in the C-terminal domain (C-NFU, 83 residues, Scheme 1) and shares significant sequence identity with Nfu in *Synechocystis Sp.*,[6] Nfu1 in yeast,[7,8] and NfuA in *Azotobacter vinelandii*,[10] all of which have been reported to be involved in the iron-sulfur cluster assembly pathway within their respective organisms. In some cases Fe-S cluster binding has been noted and a possible role as an intermediate carrier of 2Fe or 4Fe iron-sulfur clusters has been proposed. For example, the Nfu-type protein from *Synechocystis Sp* has been reported in a 2Fe-2S form[6] while *E. Coli* NfuA has also been demonstrated as an atypical carrier for 4Fe-4S clusters.[9,10] The conserved CXXC motif found in these proteins has also been identified in the C-terminal domain of NifU, the iron-sulfur cluster scaffold protein in nitrogen fixation bacterial system.[12] Overall, the factors that promote cluster binding versus alternative functional roles remain unclear. The subject of this study, human NFU, possesses a C-terminal domain (C-NFU) that contains a pair of redox active cysteines that demonstrate thioredoxin-like activity.[13,14] This domain has been shown to bind and mediate persulfide bond cleavage of sulfur-loaded IscS, the sulfide donor protein in the final step of sulfide delivery for [2Fe-2S] cluster assembly on ISU-type scaffold proteins.[15-17] Alternative mechanisms of cysteinyl persulfide cleavage by NFU have also been proposed, including direct reduction via electrons derived from ferrous ions[18] and human ferredoxin,[19] as well as a possible role for oxidized Fd in removing electrons from the nascent reduced $[2Fe\text{-}2S]^{+}$ cluster.[19]

Building from an early report,[20] protein structural flexibility has emerged as an important theme in iron-sulfur cluster biosynthesis, particularly in the chemistry of the scaffold protein that promotes cluster assembly from iron and sulfide.[20-25] Previous studies have also revealed the C-terminal domain of human NFU, another protein involved in cluster maturation, to demonstrate molten-globule-type structural behavior that may be of functional significance.[13,26,27] These studies included titration of full length and truncated constructs of NFU with 1-anilino-8-naphthalenesulfonic acid (ANS), the kinetics of trypsin digestion, and heteronuclear single-quantum coherence (HSQC) NMR spectroscopy. By contrast, the N-terminal domain (N-NFU) retains a well-defined structure.

Herein, we describe a series of studies to further advance the understanding of the structural properties and thermal stabilities of N-NFU, C-NFU, full-length NFU (NFU), as well as a mixture of N-NFU and C-NFU (N-NFU/C-NFU). These studies provide additional support for an emerging theme in the biochemistry of iron-sulfur cluster biosynthesis;[13,26,27] namely, that key parts of the protein machinery underlying Fe-S cluster assembly must display structural flexibility in order to fully execute their functions in the context of a multi-step process that could involve a variety of multi-protein complexes.[21-25,28] To advance this

investigation we have made use of differential scanning calorimetry (DSC), a thermal analytical technique that measures the heat capacity of a defined experimental sample, as well as variable temperature circular dichroism (VTCD) experiments in combination with high-field NMR spectroscopy. These bioanalytical methods not only provide information concerning the thermodynamic stability of proteins of interest, but also more detailed information on the characteristics of intermediate states involved in melting and unfolding processes.[29]

Materials and Methods

Expression and purification of human NFU

Expression and purification of human NFU was performed from BL21 Lysozyme plus (DE3) competent cells as previously described.[13,26,27] In brief, 50 mL LB culture (supplemented with 30 μg/ml kanamycin) was grown overnight followed by 1 L culture growth to an $OD_{600} \sim 0.6$ with subsequent addition of 1 mM IPTG for protein induction (3 h). The harvested cells were resuspended in Tris-buffer (50 mM Tris-HCl, pH 7.5) followed by sonication. The cell lysate was centrifuged by use of a Sorvall® RC-5B Refrigerated Superspeed Centrifuge (Du Pont Instruments) at 26,890 × *g* and 4 °C for 30 min and the resulting supernatant was loaded onto TALON® Metal Affinity Column (Clontech) equilibrated with Tris-buffer and eluted with 20 mM imidazole in Tris-buffer. The purity of the eluted protein was checked by SDS-PAGE and identity was confirmed by ESI-Mass spectrometry.

Expression of ^{15}N labeled N-terminal, C-terminal and Full Length NFU

For [^{15}N-^{1}H] HSQC analyses, $^{15}NH_4Cl$ (99%, Cambridge Isotope Laboratory) supplemented M9 minimum medium (40 mM phosphate, 22 mM Glucose, 20 mM $^{14/15}NH_4Cl$,10 mM NaCl, 2 mM $MgSO_4$, 0.1 mM $CaCl_2$, 62 μM Kanamycin) was used to express ^{15}N isotope labeled proteins. In brief, newly transformed BL21 Lysozyme plus (DE3) competent cells were grown in 20 mL of LB medium to an OD_{600} of 1.0. After centrifugation, the cell pellet was resuspended in 0.5 L of unlabeled M9 medium and grown to OD_{600} of 0.8. The resulting cells were spun down and inoculated in 2 L of labeled M9 medium and grown to OD_{600} of 0.4, followed by IPTG induction (1 mM) for 3 h. Cell harvest and protein purification steps are described above.

Differential Scanning Calorimetry

All DSC samples (0.3 mM) were dialyzed against saline phosphate buffer (40 mM Na_2HPO_4, 100 mM NaCl, pH 7.4) or phosphate buffer (40 mM Na_2HPO_4, pH 7.4) with Spectra/Por® Dialysis Membrane MWCO: 10,000 (Spectrum Laboratories, Inc). Resulting dialysis buffers were used as reference cell solvents for precision and repeatability. Prior to analyses, all sample and reference solutions were rigorously degassed with Microcal Thermovac2 (GE Healthcare). All DSC data acquisition were obtained on MicroCal VP-DSC (GE Healthcare) equipped with twin cells and operated on differential mode at a rate of 1.0 °C min^{-1} from 15 °C to 90 or 110 °C. All data were processed with Origin 7 (Origin Labs) and fit according to a Two-state model or non-two-state model with respect to individual data sets.[30]

Nuclear Magnetic Resonance Spectroscopy

[^{15}N-^{1}H] Heteroquantum Single Quantum Coherence (HSQC) spectra were recorded at The Ohio State University Campus Chemical Instrument Center. Samples (0.45 mM) were exchanged to phosphate buffer (40 mM Na_2HPO_4, 100 mM NaCl, pH 7.4) in 10% D_2O by use of an Illustra MicroSpin™ *G-25* Column (GE Healthcare). A standard water suppression

[^{15}N-^{1}H] HSQC pulse sequence was used for data collection,[31] followed by apodization, zero-filling, Fourier transformation and phase correction. Detailed acquisition and processing parameters are listed in Table S1.

Circular Dichroism Spectroscopy

All circular dichroism (CD) samples (10 μM) were dialyzed to phosphate buffer (40 mM Na_2HPO_4, pH 7.4) with Spectra/Por® Dialysis Membrane MWCO: 10,000 (Spectrum Laboratories, Inc). Resulting dialysis buffers were used as reference cell solvents for precision and repeatability. Prior to analyses, all sample and reference solutions were rigorously degassed with Microcal Thermovac2 (GE Healthcare). All CD data acquisitions were obtained on Jasco J-815 CD Spectrometer (JASCO) equipped with Quartz cells with 0.1cm path length. Secondary structure studies were collected at 8 averaging scans and 50 nm/min scan rate and monitored at 222 nm. The data were fit by K2D3 program (European Molecular Biology Laboratory).[32] Variable temperature studies were performed at a rate of 1.0 °C min^{-1} from 20 °C to 95 °C. All data were processed with Origin 7 (Origin Labs). N-NFU and C-NFU VT data were fit to equation 1 while NC-NFU and full-length NFU VT data were fit to equation 2 for T_m and ΔH_v determination:

$$\theta_{mr}=\frac{e^{\frac{1}{-RT}\times(\Delta H_v\cdot\left(1-\frac{T}{T_m}\right)-c_p\cdot\left((T_m-T)+Tln\frac{T}{T_m}\right))}}{1+e^{\frac{1}{-RT}\times(\Delta H_v\cdot\left(1-\frac{T}{T_m}\right)-c_p\cdot\left((T_m-T)+Tln\frac{T}{T_m}\right))}}\times(F-U)+U \quad (1)$$

where R is the ideal gas constant in cal/mol, T_m is the melting temperature, ΔH_v is the van't Hoff enthalpy, C_p is the heat capacity, F and U are the mean residue ellipticity (θ_{mr}) of the folded and unfolded protein, respectively,

$$\theta_{mr}=\frac{e^{\frac{1}{-RT}\times(\Delta H_{v1}\cdot\left(1-\frac{T}{T_{m1}}\right)-c_{p1}\cdot\left((T_{m1}-T)+Tln\frac{T}{T_{m1}}\right))}}{1+e^{\frac{1}{-RT}\times(\Delta H_{v1}\cdot\left(1-\frac{T}{T_{m1}}\right)-c_{p1}\cdot\left((T_{m1}-T)+Tln\frac{T}{T_{m1}}\right))}}\times(F-U_1)+\frac{e^{\frac{1}{-RT}\times(\Delta H_{v2}\cdot\left(1-\frac{T}{T_{m2}}\right)-c_{p2}\cdot\left((T_{m2}-T)+Tln\frac{T}{T_{m2}}\right))}}{1+e^{\frac{1}{-RT}\times(\Delta H_{v2}\cdot\left(1-\frac{T}{T_{m2}}\right)-c_{p2}\cdot\left((T_{m2}-T)+Tln\frac{T}{T_{m2}}\right))}}\times(U_1-U_2)+U_2 \quad (2)$$

where the subscripts of T_m, ΔH_v and C_p denote the transition parameters associated with the C-terminal and N-terminal domain, respectively.

Results

DSC Studies of N-Terminal Human NFU

N-NFU DSC analyses were found to be in agreement with our previous NMR and CD studies[27] inasmuch as N-NFU displays a rigid, well-behaved native structure at ambient temperature (Figure 1). The melting curve was analyzed and fit to a two peak non-two state model, yielding physical constants for melting temperatures (T_m) of 74.7 ± 0.6 and 78.4 ± 0.1 °C (Table 1). The changes in molar enthalpy (ΔH_{cal}) and van't Hoff enthalpy (ΔH_υ) from the fitting parameters were determined to be 134.6 ± 9.9 kcal/mol, and 141.4 ± 4.2 kcal/mol for the lower transition and 93.2 ± 9.8 kcal/mol, and 79.2 ± 1.6 kcal/mol for the higher transition, respectively (Table 2). The high T_m indicates the unfolding transitions for N-NFU to stem from a well-folded state, while the reproducibility of melting for a sample following repetition of the heating cycle indicates that the melting process is reversible, but with partial protein degradation arising during each cycle (Figure S1). This evidence suggests that

at high temperature the N-NFU domain exists in a stable conformation, and is able to fold back to the native state upon cooling.

VTCD Studies of N-Terminal Human NFU

The secondary structure of N-NFU was analyzed by CD spectroscopy and yielded a composition of 31% α -helix, 21% β -sheet and 48% random coil (Table 3). The K2D3 program[32] was used to obtain a more accurate prediction of secondary structure composition than was previously possible.[13] Variable temperature studies yielded a structural transition at T_m = 79.5 ± 0.4 °C with ΔH_υ = 69.6 ± 6.1 kcal/mol (Figure 2, Tables 4 and 5), which is consistent with DSC results for secondary structure loss at 3.7 °C higher than the tertiary structure transition (Table 1).

DSC Studies of C-Terminal Human NFU

DSC analyses of the C-terminal domain of human NFU were consistent with a molten globule-like native structure[27] as the melting curve was observed to be broad and asymmetric over a span of 43 °C (Figure 3, top). Four transitions were calculated from the melting curve using the non-two-state model, with T_m's ranging from 55.0 °C to 72.9 °C. The first transition curve was observed to be broad, with $\Delta H_{cal} > \Delta H_\upsilon$ in agreement with a molten globule-like native state structure. As the temperature increased, the calculated melting curves became sharper, resulting in $\Delta H_{cal} < \Delta H_\upsilon$ for the transition at 72.9 °C. In conjunction with a negative peak observed at 74 °C, the transitions at 70.0 °C and 72.9 °C suggest protein aggregation at elevated temperature. As expected, due to the structural instability of C-NFU, the melting and refolding cycle was irreversible as opposed to its N-NFU counterpart, and denatured precipitate was observed after a single heating ramp.

VTCD Studies of C-Terminal Human NFU

The thermal melting profile of the C-NFU secondary structure was monitored over the entire scanning range, from 20 °C to 95 °C (Figure 3, bottom, and Tables 4 and 5). The overall CD signal change was determined to be 5.9 ± 0.2 mdeg. This is consistent with the DSC results that supported the low overall thermal stability of the C-NFU structure, which denatures over a broad range between 50 °C ∼ 80 °C. Furthermore, the constant decrease of secondary structure (222 nm) over the entire heat ramp indicates multiple intermediates during melting, which is also consistent with DSC results using a four-state fitting model to define the structural loss. A single transition fit of the C-NFU melt resulted in a relatively low ΔH_ν (13.6 ± 3.2 kcal/mol), further indicating the absence of a distinct native-state secondary structure.

DSC and VTCD Studies of Full Length Human NFU

Two distinct secondary transitions were observed in VTCD profiles of NFU (Figure 4, bottom, and Tables 4 and 5). The transition at 77.8 ± 0.9 °C is tentatively assigned to the N-terminal domain due to the similarity in T_m in comparison to the N-NFU domain alone. The lower transition at 67.8 ± 0.8 °C is likely due to the unfolding of the C-terminal domain, since it corresponds to the lowest thermally stable domain for NFU. The van't Hoff energies associated with the N-terminal and C-terminal domains were determined to be 41.0 ± 2.7 and 23.9 ± 1.7 kcal/mol, respectively. The distinct transition observed for the C-terminal domain at its T_m, together with the increased melting ΔH_ν relative to C-NFU alone, suggests that the secondary structure of this domain is stabilized in NFU.

The thermal melting curve of NFU (Figure 4, top) indicates a convoluted transition with T_m near 72 °C. Using the secondary structure unfolding ΔH_v determined by the VTCD, the DSC plot was fit to four peaks that correspond to the loss of secondary and tertiary structure of

the N- and C-domains of the NFU. In comparison with the DSC melting curves from the N-terminal domain (Figure 1) and the C-terminal domain (Figure 3, top), two of four peaks of the NFU melting curve correspond to the individual domains of the full length protein; the higher T_m of 77.1 ± 3.7 °C corresponds to melting of the N-NFU domain whereas the lower T_m of 67.0 ± 0.3 °C corresponds to unfolding of the C-NFU domain. The relatively modest difference between ΔH_{cal} and $\Delta H_{\upsilon H}$ for both transitions is characteristic of a two-state unfolding processes, suggesting the absence of melting intermediates or protein aggregation of the individual domains in the full length protein. Furthermore, the similarity of the two enthalpies in NFU compared with the individual domains, along with the reversibility of melting (Figure S1), suggests that in forming the full length protein, both domains have been structurally stabilized. These changes in thermodynamic and structural properties are more significant for the C-NFU domain, as forming the complete protein apparently alters its native state and results in a relatively more structurally-ordered macromolecule. The C-NFU domain in NFU is thermally well-behaved as the fitting yielded an overall melting ΔH_{cal} of 114.1 ± 10.8 kcal/mol (Table 2). We speculate that in the full length protein, the C-terminal domain is stabilized by the N-terminal domain and therefore exhibits significant tertiary structure in comparison to the isolated domain.

DSC Studies of a Mixture of N- and C-Terminal Domains of NFU

The DSC results described thus far demonstrate unusual, but interesting interactions between the N- and C-terminal domains of NFU. To further elucidate the chemistry between the two segments we carried out DSC studies on solution mixtures of equimolar N-NFU and C-NFU (Figure 5, top), which yielded three noteworthy observations. First, the transitions at T_m's of 49.3 ± 0.3 and 58.1± 0.4 °C correspond to unfolding of C-NFU in the solution mixture. The overall structural behavior of C-NFU in the presence of N-NFU was observed to be more stable, with a symmetric melting profile and $\Delta H_{cal} \approx \Delta H_{\upsilon}$. Furthermore, the secondary and tertiary structural T_m's observed for C-NFU in solution with N-NFU are 8.93 ± 0.5 and 14.04 ± 3.4 °C lower than that of the C-NFU domain of the full-length NFU protein, respectively, indicating that the degree of structural stabilization by N-NFU is stronger when the two domains are covalently attached. The interaction surface between the two domains is likely to be dominated by hydrophobic interactions, since decreasing buffer ionic strength was observed to weaken the degree of thermal stabilization of C-NFU. This is consistent with the results of isothermal titration calorimetry studies where no significant enthalpic response was observed by titrating the two domains.[13] Rather, any binding would have to be promoted by entropy-driven interactions. Lastly, interaction between the two domains increases the overall structural stability of the N-terminal domain, which can be observed from the increased T_m and an overall increase of 129.7 ± 14.1 kcal/mol in molar enthalpy.

VTCD Studies of a Mixture of N- and C-Terminal Domains of NFU

Similar to NFU, the VTCD melting curve of a mixture of N-NFU and C-NFU showed two distinct transitions (Figure 5, bottom, and Table 4). The lower transition was observed at 59.2 ± 0.5 °C and corresponds to the C-NFU secondary structure melt. In comparison to the VTCD profile for C-NFU alone, the thermal transition was observed to be well behaved with ΔH_v = 43.3 ± 4.1 kcal/mol in the presence of N-NFU (Table 5), which is more than three-fold larger than the C-NFU-only VTCD melting curve. The thermodynamic parameters evaluated for C-NFU are in agreement with its DSC profile and estimated melting enthalpies, and support the conformational change and structural stabilization of C-NFU following binding to N-NFU.

[^{15}N-^{1}H] HSQC Studies of a Mixture of N- and C-Terminal Domains of NFU

To further study the interaction between N-NFU and C-NFU, each of the two domains was prepared in an ^{15}N-isotopically-enriched form. First, comparing the spectra from the isolated ^{15}N-N-NFU domain, and either an equimolar mixture of ^{15}N-N-NFU and ^{14}N-CNFU, or the ^{15}N-labeled full length protein (Figure S8) revealed no shifted cross-peaks and no significant change in the conformation of the N-terminal domain. That is the structure appears conserved for both the isolated N-NFU, in complex with C-NFU, and as a separate domain in the full-length NFU protein. By contrast, experiments conducted with the C-terminal C-NFU domain under the same solution conditions as the DSC analyses demonstrated very distinct behavior. When equimolar mixtures of ^{14}N-N-NFU and ^{15}N-C-NFU were mixed and studied by [^{15}N-^{1}H] HSQC NMR experiments, a comparison of the spectrum relative to that obtained for the isolated ^{15}N-labeled C-NFU domain revealed 21 new ^{15}N-^{1}H cross-peaks (Figures 6A and 6B, Table S2). These peaks suggest an alternative tertiary conformation for C-NFU following interaction with the N-NFU domain. Furthermore, the observed new peaks exhibit distinct chemical shifts that span the chemical shift range from 6.67 to 9.96 ppm in the ^{1}H domain, and from 103.98 to 130.27 ppm in the ^{15}N domain, supporting a conformational change in C-NFU with a greater level of tertiary structure and corresponding diversity in the chemical environment of its residues. When the spectrum for the ^{15}N-labeled C-NFU domain was compared to that for the ^{15}N-labeled full-length NFU (Figures 6A and 6C) a total of 23 new cross-peaks were observed (Table S3). Significantly, only 4 of those new cross-peaks found for C-NFU in the full length NFU protein were co-localized with cross-peaks observed in the spectrum for the mixture of the ^{14}N-N-NFU and ^{15}N-C-NFU domains (Table S3, bold). Apparently the structural transition induced by complex formation between the isolated N-NFU and C-NFU domains is incomplete, relative to the two domains in the full-length NFU protein

Discussion

Comparison of the two isolated domains of the full-length NFU protein has shown the N-terminal fragment to display higher thermal stability relative to its C-NFU counterpart (Figure 1 and Figure 3, top, respectively). This is consistent with our previous studies demonstrating the N-terminus of NFU to possess a more rigid conformation than the C-terminal NFU.[27] The C-terminal domain exhibits molten globule characteristics with lower thermostability (Figure 3, bottom) and does not display a well-folded tertiary structure according to both CD and NMR criteria.[13,26,27] DSC studies of C-NFU reported herein displayed structural heterogeneity during the unfolding process (Figure 3, top), while the VTCD melt showed a consistent decrease in secondary structure throughout the temperature domain (Figure 3, bottom). The ability of N-NFU to promote conformational change and stabilize the structure of C-NFU was confirmed by both DSC and CD melting experiments (Figure 5) and 2D-NMR experiments (Figure 6). The degree of stabilization was observed to be greater for full-length NFU, relative to a mixture of the two domains (Figure 6B vs. 6C). The secondary structures of the N-NFU/C-NFU mixture contain 2% less random coil than the expected composition, which is consistent with the sharp CD melting curve due to the new C-NFU conformation (Figure 5, bottom). Although N-NFU somewhat stabilizes the secondary and tertiary structure of C-NFU, there remains a significant amount of molten globular C-NFU within the mixture of the two proteins, with 50% random coil present in the secondary structure (Table 3). Increasing ionic strength is known to stabilize the thermostability of molten globules.[33] Accordingly, the difference in the degree of structural stabilization between these two cases is also reflected in the results of DSC studies using a lower ionic strength buffer (0 mM NaCl), where a decrease of 18.6 °C was observed in the T_m for C-NFU in the mixture of proteins, but only by 10.5 °C in NFU (Table 1). Furthermore, by comparing the [^{15}N-^{1}H] HSQC NMR spectrum of full-length NFU relative

to that from a mixture of the N-NFU and C-NFU domains, 23 new cross peaks were observed (Figures 6C and S7), relative to the 21 new peaks observed for C-NFU following N-NFU binding in the co-complex of the two domains (Figures 6B and S6), although only 4 of these new cross-peaks from each spectrum are found to co-localize (Tables S2 and S3). These residues underline the difference between the N/C-domain protein-protein interaction and covalently attached NFU. Nevertheless, the ability of N-NFU to structurally stabilize C-NFU was demonstrated in both cases through the appearance of new cross peaks in the NMR experiments (Figure 6) and is consistent with the progressive changes observed in the DSC plots for each isolated domain, relative to the mixture of domains and full-length protein (Figures 1 to 5).

The Gibbs free-energy for the secondary structural transition was converted from CD melt data by using equation 3 and drawn to illustrate the unfolding profile for N-NFU (Figure 7).

$$\Delta G = -RT \cdot \ln \frac{\theta_{mr} - U}{F - \theta_{mr}} \quad (3)$$

According to the plot, as temperature increases, the ΔG response is first observed to increase as the melting process is enthalpy driven. The free energy ΔG reaches the highest value at ∼ 37 °C, since N-NFU is most likely thermostable at physiological temperatures. The unfolding free energy decreases from 37 to 78 °C, because the unfolding process is entropy driven. Figure 8 shows the thermal profile of a mixture of N- and C-NFU, and NFU, to be similar to the N-NFU thermal profile, where all thermal transitions were fit to yield a ΔG_{max} near 37 °C.

The influence of N-NFU on C-NFU underlines the importance of the structural role of the N-terminal domain on the native structure of NFU. In agreement with our previous studies, the N-terminal domain appears to maintain the overall structure of the full-length protein.[13,26,27] We conclude that hydrophobic interactions between the N- and C-terminal domains facilitate the folding of each, illustrated by the observation that the unfolding of C-NFU changes from a molten globule state to a relatively more thermally stable conformation. However, the C-terminal domain in the full-length protein is not fully structured as observed by NMR experiments.[27] This is also supported by the increased thermostability of the C-terminal domain under high salt conditions. Structural disorder is generally considered to be a factor that decreases enzyme catalytic efficiency. However, recent reports have shown molten globular enzymes adopting functional conformations upon binding to relevant binding partners or ligands, such as the case of chorismate mutase.[34] Similarly, the molten globular C-terminal domain of NFU may adopt its functional conformation upon binding to sulfur donors and subsequently aid in the 2Fe2S cluster assembly with scaffolding proteins. As demonstrated by both ITC and kinetic studies, human NFU is known to bind to IscS in the process of reconstitution of human ISU scaffold protein.[13] In order for the conserved CXXC thiolate groups to reduce the persulfide bond on IscS and subsequent relocation of sulfide ions into the ISU active site, it is likely that the C-NFU adopts a distinct and more structured conformation. The absence of a thermally stable tertiary conformation for the C-terminal CXXC domain may provide the required structural flexibility to allow such a reaction. The decrease in flexibility of C-NFU in the presence of N-NFU was also observed in the secondary structure predictions, with an increase in ∼2% α -helix content (5 residues) upon binding. A recent bioinformatic study reported that the majority of protein-protein interaction are due to helix interactions (62%) with involvement commonly between 4 to 14 residues,[35] such as the bacterial Bernase-Barstar system.[36] The Zimm-Bragg theory describes that the rate determining step in formation of α -helix is the formation of the first loop, which requires ∼20 kcal. However, the subsequent helix growth

is exothermic and a thermodynamically favored process. Therefore, the formation of additional alpha helix content between the two terminals of NFU is likely to be entropy driven and forms spontaneously, leading to an alternative secondary and tertiary conformation for the C-terminal domain.

Conclusion

The term molten globule is ascribed to a diverse category of protein structural conformations that are broadly defined by a high degree of secondary structure, but lacking a rigid tertiary structure.[37,38] There are many examples for alternative conformers with distinct recognition or functional roles within a given protein molecule.[39-41] Calorimetry results and our previous investigations[13,27] suggest the C-terminal domain of human NFU to exist in a molten globule state in both the truncated form and within the full-length protein, but with different conformations and physical properties. The C-terminal domain appears to adopt an alternative conformation following interaction with the N-terminal domain. This change in conformation is accompanied by an increase in the tertiary structure, as well as an increase in thermostability. This property of structural flexibility most likely underlies the required properties and functions of the protein, as also observed in the cases of molten globular clusterin and nucleosomes.[42] Interestingly, the iron-sulfur scaffold protein *T. maritima* IscU appears to equilibrate between structural conformers, and may be essential for its interactions with various protein partners.[20] Structural isomerism within this family of scaffold proteins has also been emphasized by recent work from the Markley group.[21-25] Due to the complexity of iron-sulfur cluster assembly systems, and numerous contributions from scaffold, partner and chaperone proteins, we propose that a dynamic tertiary structure is an important factor for the proper functioning of several key protein involved with Fe-S cluster formation.

Supplementary Material

Refer to Web version on PubMed Central for supplementary material.

Acknowledgments

Funding: This work was supported by a grant from the National Institutes of Health [AI072443].

References

1. Lorain S, Lecluse Y, Scamps C, Mattei MG, Lipinski M. Identification of human and mouse HIRA-interacting protein-5 (HIRIP5), two mammalian representatives in a family of phylogenetically conserved proteins with a role in the biogenesis of Fe/S proteins. Biochim Biophys Acta. 2001; 1517:376–383. [PubMed: 11342215]
2. Magnaghi P, Roberts C, Loraine S, Lipinski M, Scambler PJ. HIRA, a mammalian homologue of Saccharomyces cerevisiae transcriptional co-repressors, interacts with Pax3. Nat Genet. 1998; 20:74–77. [PubMed: 9731536]
3. Ganesh S, Tsurutani N, Suzuki T, Ueda K, Agarwala KL, Osada H, Delgado-Escueta AV, Yamakawa K. The Lafora disease gene product laforin interacts with HIRIP5, a phylogenetically conserved protein containing a NifU-like domain. Hum Mol Genet. 2003; 12:2359–2368. [PubMed: 12915448]
4. Tong WH, Jameson GN, Huynh BH, Rouault TA. Subcellular compartmentalization of human Nfu, an iron—sulfur cluster scaffold protein, and its ability to assemble a [4Fe–4S] cluster. Proc Natl Acad Sci USA. 2003; 100:9762–9767. [PubMed: 12886008]
5. Nishio K, Nakai M. Transfer of Iron-Sulfur Cluster from NifU to Apoferredoxin. J Biol Chem. 2000; 275:22615–22618. [PubMed: 10837463]

6. Nakamura Y, Kaneko T, Hirosawa M, Miyajima N, Tabata S. CyanoBase, a www database containing the complete nucleotide sequence of the genome of Synechocystis sp. strain PCC6803. Nucl Acids Res. 1998; 26:63–67. [PubMed: 9399802]
7. Schilke B, Voisine C, Beinert H, Craig E. Evidence for a conserved system for iron metabolism in themitochondria of Saccharomyces cerevisiae. Proc Natl Acad Sci U S A. 1999:10206. [PubMed: 10468587]
8. Garland SA, Hoff K, Vickery LE, Culotta VC. Saccharomyces cerevisiae ISU1 and ISU2: members of a well-conserved gene family for iron-sulfur cluster assembly. J Mol Biol. 1999; 294:897–907. [PubMed: 10588895]
9. Py B, Gerez C, Angelini S, Planel R, Vinella D, Brochier-Amanet C, Serres RG, Latour JM, Choudens SO, Fontecave M, Barras F. Molecular organization, bichemical function, cellular role and evolution of NfuA, an atypical Fe-S carrier. Molecular Microbiology. 2012; 86:155–171. [PubMed: 22966982]
10. Bandyopadhyay S, Naik SG, O'Carroll IP, Huynh BH, Dean DR, Johnson MK, Dos Santos PC. A proposed role for the Azotobacter vinelandii NfuA protein as an intermediate iron-sulfur cluster carrier. J Biol Chem. 2008; 283:14092–14099. [PubMed: 18339629]
11. Liu Y, Cowan JA. Iron sulfur cluster biosynthesis. Human NFU mediates sulfide delivery to ISU in the final step of [2Fe-2S] cluster assembly. Chem Commun. 2007:3192–3194.
12. Yuvaniyama P, Agar JN, Cash VL, Johnson MK, Dean DR. NifS-directed assembly of a transient [2Fe–2S] cluster within the NifU protein. Proc Natl Acad Sci USA. 2000; 97:599–604. [PubMed: 10639125]
13. Liu Y, Qi W, Cowan JA. Iron-sulfur cluster biosynthesis: functional characterization of the N- and C-terminal domains of human NFU. Biochemistry. 2009; 48:973–980. [PubMed: 19146390]
14. Frazzon J, Fick JR, Dean DR. Biosynthesis of iron-sulphur clusters is a complex and highly conserved process. Biochem Soc Trans. 2002; 30:680–685. [PubMed: 12196163]
15. Dean DR, Bolin JT, Zheng LM. Nitrogenase Metalloclusters - Structures, Organization, and Synthesis. Journal of Bacteriology. 1993; 175:6737–6744. [PubMed: 8226614]
16. Gerber J, Muhlenhoff U, Lill R. An interaction between frataxin and Isu1/Nfs1 that is crucial for Fe/S cluster synthesis on Isu1. EMBO Rep. 2003; 4:906–911. [PubMed: 12947415]
17. Mansy SS, Cowan JA. Iron-sulfur cluster biosynthesis: toward an understanding of cellular machinery and molecular mechanism. Acc Chem Res. 2004; 37:719–725. [PubMed: 15379587]
18. Muhlenhoff U, Richhardt N, Gerber J, Lill R. Characterization of iron-sulfur protein assembly in isolated mitochondria. A requirement for ATP, NADH, and reduced iron. J Biol Chem. 2002; 277:29810–29816. [PubMed: 12065597]
19. Li J, Saxena S, Pain D, Dancis A. Adrenodoxin Reductase Homolog (Arh1p) of Yeast Mitochondria Required for Iron Homeostasis. J Biol Chem. 2001; 276:1503. [PubMed: 11035018]
20. Mansy SS, Wu SP, Cowan JA. Iron-Sulfur Cluster Biosynthesis: Biochemical characterization of the conformational dynamics of Thermotoga maritima IscU and the relevance for cellular cluster assembly. J Biol Chem. 2004; 279:10469–10475. [PubMed: 14688265]
21. Dai Z, Tonelli M, Markley JL. Metamorphic protein IscU changes conformation by cis-trans isomerizations of two peptidyl-prolyl peptide bonds. Biochem. 2012; 51:9595–9602. [PubMed: 23110687]
22. Fuzery AK, Oh JJ, Ta DT, Vickery LE, Markley JL. Three hydrophobic amino acids in Escherichia coli HscB make the greatest contribution to the stability of the HscB-IscU complex. BMC Biochem. 2011; 12:1–9. [PubMed: 21205312]
23. Kim JH, Tonelli M, Frederick RO, Chow DCF, Markley JL. Specialized Hsp70 Chaperone (HscA) Binds Preferentially to the Disordered Form, whereas J-protein (HscB) Binds Preferentially to the Structured Form of the Iron-Sulfur Cluster Scaffold Protein (IscU). J Biol Chem. 2012; 287:31406–31413. [PubMed: 22782893]
24. Kim JH, Tonelli M, Markley JL. Disordered form of the scaffold protein IscU is the substrate for iron-sulfur cluster assembly on cysteine desulfurase. Proc Natl Acad Sci USA. 2012; 109:454–459. [PubMed: 22203963]

25. Markley JL, Kim JH, Dai Z, Bothe JR, Cai K, Frederick RO, Tonelli M. Metamorphic protein IscU alternates conformations in the course of its role as the scaffold protein for iron-sulfur cluster biosynthesis and delivery. FEBS Lett. 2013 Ahead of Print.
26. Liu Y, Cowan JA. Iron sulfur cluster biosynthesis. Human NFU mediates sulfide delivery to ISU in the final step of [2Fe-2S] cluster assembly. Chem Commun (Camb). 2007:3192–3194. [PubMed: 17653385]
27. Liu Y, Cowan JA. Iron-sulfur cluster biosynthesis: characterization of a molten globule domain in human NFU. Biochemistry. 2009; 48:7512–7518. [PubMed: 19722697]
28. Cowan JA. Iron sulfur cluster biosynthesis: scaffold and donor proteins, and mechanistic insights. ACS Symposium Series. 2009; 1012:3–16.
29. Spink CH. Differential scanning Calorimetry. Biophysical Tools for Biologists: Vol 1 in Vitro Techniques. 2008; 84:115–141.
30. Sturtevant JM. Biochemical Applications of Differential Scanning Calorimetry. Annual Review of Physical Chemistry. 1987; 38:463–488.
31. Mori S, Abeygunawardana C, O'Neil-Johnson M, van Zijl PCM. Improved sensitivity of HSQC spectra of exchanging protons at short interscan delays using a new fast HSQC (FHSQC) detection scheme that avoids water saturation. J Magn Reson B. 1995; 108:94–98. [PubMed: 7627436]
32. Louis-Jeune C, Andrade-Navarro MA, Perez-Iratxeta C. Prediction of protein secondary structure from circular dichroism using theoretically derived spectra. Proteins. 2011; 80:374–381.
33. Nishii I, Kataoka M, Goto Y. Thermodynamic stability of the molten globule states of apomyoglobin. J Mol Biol. 1995; 250:223–238. [PubMed: 7608972]
34. Pervushin K, Vamvaca K, Vogeli B, Hilvert D. Structure and dynamics of a molten globular enzyme. Nat Struct Mol Biol. 2007; 14:1202–1206. [PubMed: 17994104]
35. Jochim AL, Paramjit SA. Assessment of helical interfaces in protein-protein interactions. Mol BioSyst. 2009; 5:924–926. [PubMed: 19668855]
36. Buckle AM, Schreiber G, Fersht AR. Protein-protein recognition: crystal structural analysis of a barnase-barstar complex at 2.0-A resolution. Biochem. 1994; 33:8878–8889. [PubMed: 8043575]
37. Ohgushi M, Wada A. 'Molten-globule state': a compact form of globular proteins with mobile side-chains. FEBS Lett. 1983; 164:21–24. [PubMed: 6317443]
38. Kuwajima K. A folding model of α-lactalbumin deduced from the three-state denaturation mechanism. J Mol Biol. 1977; 114:241–258. [PubMed: 909087]
39. Wilson G, Ford SJ, Cooper A, Hecht L, Wen ZQ, Barron LD. Vibrational Raman optical activity of α -lactalbumin: comparison with lysozyme, and evidence for native tertiary folds in molten globule states. J Mol Biol. 1995; 254:747–760. [PubMed: 7500347]
40. Fink AL. Compact intermediate states in protein folding. Annu Rev Biophys Biomol Struct. 1995; 24:495–522. [PubMed: 7663125]
41. Creighton TE. Protein folding. Biochem. 1990; 270:1–16.
42. Dunker AK, Lawson JD, Brown CJ, Williams RM, Romero P, Oh JS, Oldfield CJ, Campen AM, Ratliff CM, Hipps KW, Ausio J, Nissen MS, Reeves R, Kang C, Kissinger CR, Bailey RW, Griswold MD, Chiu W, arner EC, Obradovic Z. Intrinsically disordered protein. J Mol Graph Model. 2001; 19:26–59. [PubMed: 11381529]

Abbreviations

ANS	1-anilino-8-naphthalenesulfonic acid
CD	Circular Dichroism
DSC	differential scanning calorimetry
HIRA	histone cell cycle regulation homolog A
IPTG	isopropyl-β-D-thiogalactopyranoside
HSQC	heteronuclear single-quantum coherence

Isc	iron sulfur cluster
ITC	isothermal titration calorimetry
LB	Luria-Bertani
MWCO	molecular weight cut off
PAGE	Polyacrylamide Gel Electrophoresis
Tris	Tris (hydroxymethyl)aminomethane
VTCD	variable temperatire circular dichroism

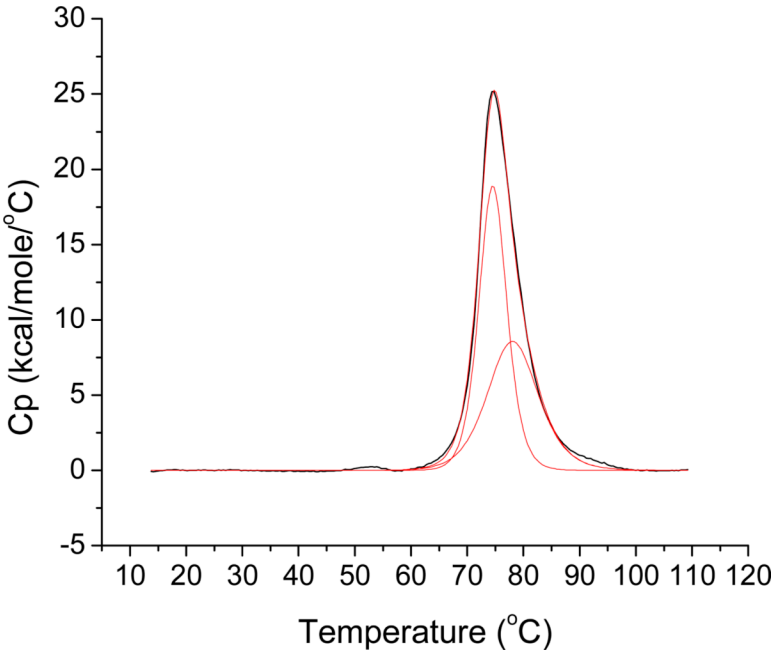

Figure 1.

Differential scanning calorimetry profile for a 0.3 mM N-NFU solution in phosphate buffer. Origin was used to fit the data to a 2-peak, non-2-state model (MN2State). Values for T_m, ΔH_{cal} and $\Delta_v H$ were obtained from the fit and are listed in Tables 1 and 2. The lower melting point was initialized at 79.4 °C, which was obtained from a VTCD analysis.

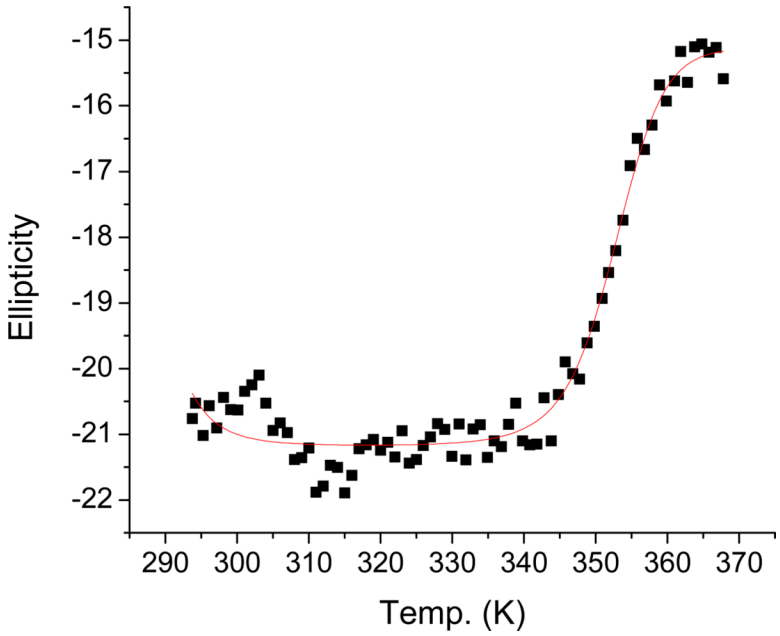

Figure 2.

VTCD analysis of 10 μM N-NFU in 40 mM phosphate 100 mM NaCl buffer. Data were fit to equation 1 to yield values of ΔH_{υ}, T_m^{sec}, and ΔC_p of 69.56 kcal/mol, 79.44 °C and 2.02 kcal/mol.K, respectively. Ellipticity data was directly used without converting to molar ellipticity units because the van't Hoff enthalpies are independent of such a factor. T_m^{sec} was used as an initial value for T_m in the DSC data fitting routine.

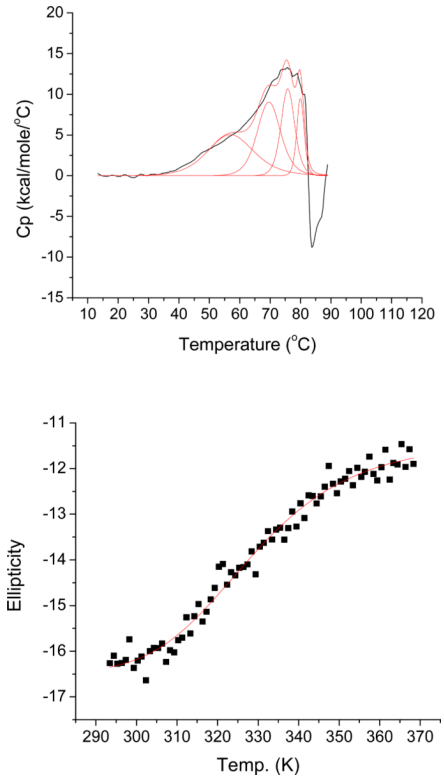

Figure 3.

DSC and VTCD analysis of C-NFU in 40 mM phosphate 100 mM NaCl buffer. (Top) Upscan of 0.3 mM C-NFU from 10 °C to 90 °C with rate of 1 K/min recorded by DSC. (Bottom) Upscan of 10 μM C-NFU with the same conditions monitored at 222 nm by CD. VTCD data were fit to equation 1 and results are listed in Tables 4 and 5. Fitting results from DSC experiments are listed in Tables 1 and 2.

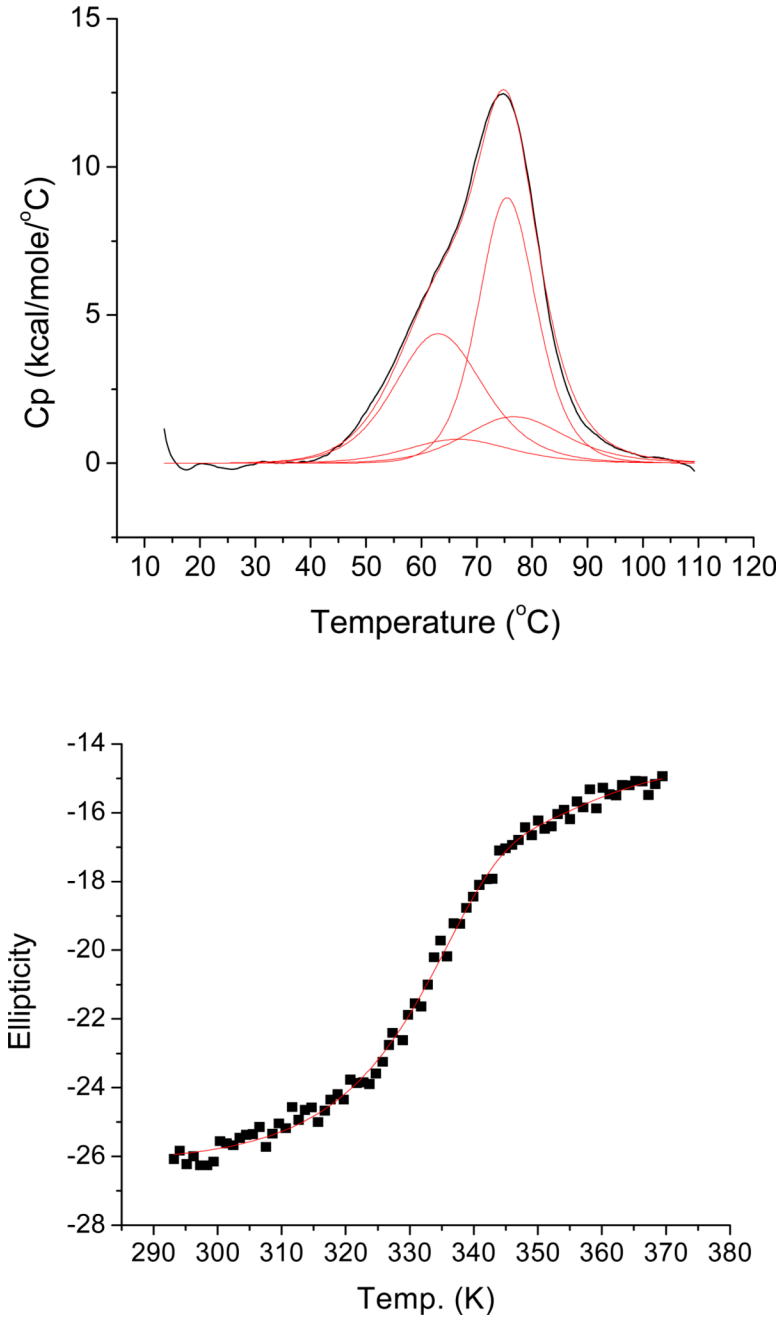

Figure 4.

DSC and VTCD analysis of NFU in 40 mM phosphate 100 mM NaCl buffer. (Top) Upscan of 0.3 mM NFU from 10 °C to 110 °C at a rate of 1 K/min recorded by DSC. (Bottom) Upscan of 10 μM NFU under the same conditions, but monitored at 222 nm by CD. VTCD data were fit to equation 2 and results are listed in Tables 4 and 5. Fitting results from DSC experiments are listed in Tables 1 and 2.

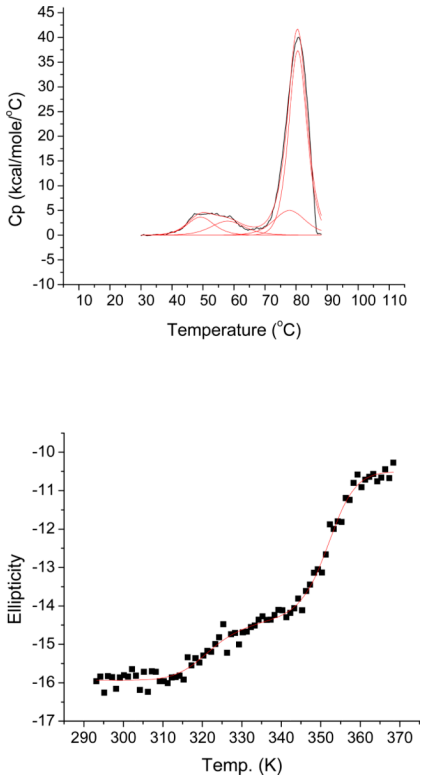

Figure 5.
DSC and VTCD analysis of a N-NFU / C-NFU mixture in 40 mM phosphate 100 mM NaCl buffer. (Top) Upscan of a mixture of 0.3 mM N-NFU and C-NFU from 10 °C to 90 °C at rate of 1 K/min recorded by DSC. (Bottom) Upscan of a 10 μM mixture of 0.3 mM N-NFU and C-NFU under the same conditions, but monitored at 222 nm by CD.

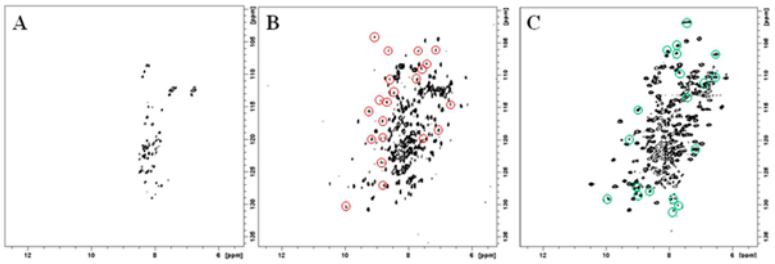

Figure 6.

^{1}H-^{15}N HSQC spectra of (A) ^{15}N-C-NFU, (B) [^{14}N-N-NFU + ^{15}N-C-NFU] and (C) ^{15}N-NFU. The C-terminal domain undergoes structural change in the presence of the N-terminal domain, as reflected by the peaks circled in red in (B). Cross peaks are also observed in spectrum (B) from the non-enriched N-NFU domain as a result of natural abundance ^{15}N and provide an effective comparison of spectra for full-length NFU (C) relative to the sum of the individual domains (B). The cross-peaks circled in green in spectrum (C) highlight the chemical shifts of the full-length protein that are unique from the individual domains and in some cases overlaps with the peaks from the structure stabilized C-terminal domain. Chemical shifts for new cross-peaks identified in (B) and (C) are listed in Tables S2 and S3, respectively.

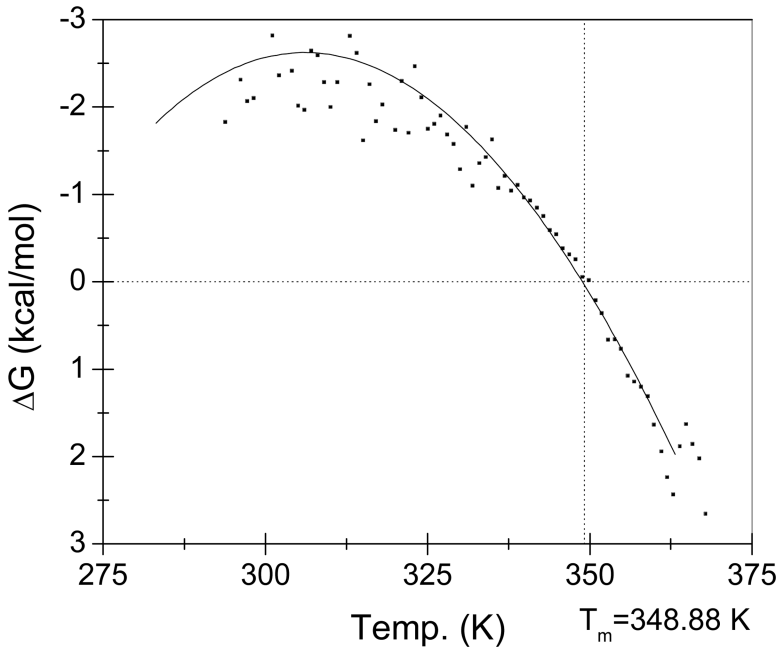

Figure 7.

Thermal profile for N-NFU. Data (dots) were converted to ΔG values by use of equation (3), and the Gibbs-Helmholtz equation, along with ΔH_{υ}, T_m^{sec}, and ΔC_p, was used to form a plot of ΔG versus temperature (line). As expected, N-NFU is most thermally stable near human body temperature while melting of the protein is a favorable process at temperatures exceeding 79.4 °C.

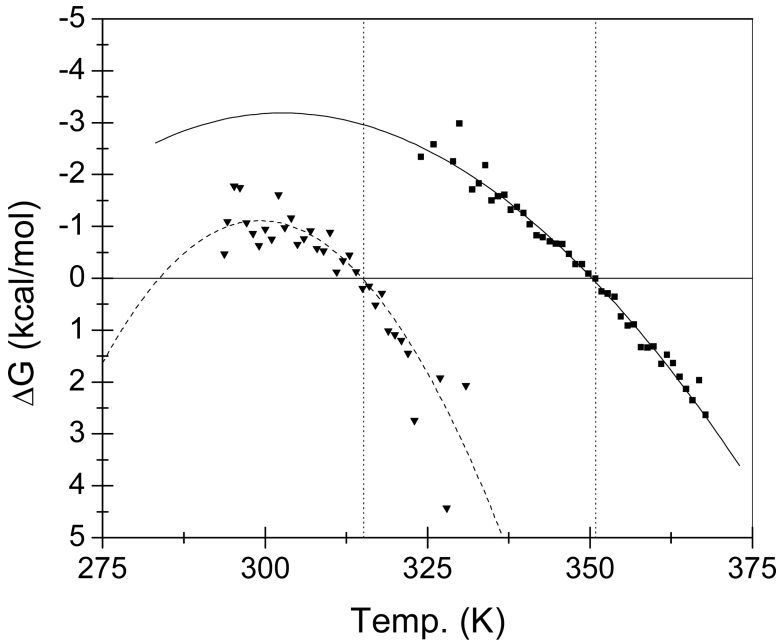

Figure 8.

Gibbs free energy plot illustrates a mixture of N-NFU and C-NFU domains to be most thermally stable near physiological temperature. The solid line represents the calculated data for N-NFU, and the dashed line the calculated data for C-NFU. Squares show the experimental data for N-NFU, and triangles show the experimental data for C-NFU. The vertical dashed lines indicate the fitted T_m's of C-NFU (315.0 K) and N-NFU (350.3 K).

```
1    GSSHHHHHHS SGLVPRGSHM FIQTQDTPNP NSLKFIPGKP VLETRTMDFP TPAAAFRSPL
61   ARQLFRIEGV KSVFFGPDFI TVTKENEELD WNLLKPDIYA TIMDFFASGL PLVTEETPSG
121  EAGSEEDDEV VAMIKELLDT RIRPTVQEDG GDVIYKGFED GIVQLKLQGS CTSCPSSIIT
181  LKNGIQNMLQ FYIPEVEGVE QVMDDESDEK EANSP
```

Scheme 1.

NFU sequence showing the N-terminal domain in bold and the C-terminal domain underlined.

Table 1

Melting temperatures for N-terminal NFU, C-terminal NFU, a mixture of N- and C-terminal domains, and full-length NFU determined by DSC.

	[NaCl] (mM)	T_{m1} (°C)	T_{m2} (°C)	T_{m2} -T_{m1} (°C)	T_{m3} (°C)	T_{m4} (°C)	T_{m4} -T_{m3} (°C)
N-NFU	100.0	74.7 ± 0.6	78.4 ± 0.1	3.7	-	-	-
	0.0	75.0 ± 0.6	80.0 ± 0.1	5.1	-	-	-
C-NFU	100.0	57-80	57-80	-	-	-	-
	0.0	49-81	49-81	-	-	-	-
N-NFU / C-NFU	100.0	49.3 ± 0.3	58.1 ± 0.4	8.8	78.0 ± 1.5	80.6 ± 0.2	2.6
	0.0	28.7 ± 0.7	41.4 ± 0.7	12.7	76.6 ± 0.5	80.9 ± 0.1	4.3
NFU	100.0	63.3 ± 3.4	67.0 ± 0.3	3.7	75.6 ± 7.9	77.1 ± 3.7	1.5
	0.0	51.3 ± 0.6	58.1 ± 2.6	6.7	69.4 ± 4.9	76.1 ± 1.2	6.7

For a well-folded N-terminal domain, the change in melting temperatures for secondary and tertiary structures Δ (T_m^{ter}-T_m^{sec}) is inversely related to the ionic strength. The majority of this observation is contributed by the decrease in T_m^{sec} at lower ionic strength.

Table 2

ΔH_{cal} and ΔH_v for N-terminal NFU, C-terminal NFU, a mixture of N- and C-terminal domains, and full-length NFU determined by DSC.

	[NaCl] (mM)	$\Delta H_{cal\ 1}$ (kcal mol^{-1})	ΔH_{v1} (kcal mol^{-1})	$\Delta H_{cal\ 2}$ (kcal mol^{-1})	ΔH_{v2} (kcal mol^{-1})	$\Delta H_{cal\ 3}$ (kcal mol^{-1})	ΔH_{v3} (kcal mol^{-1})	$\Delta H_{cal\ 4}$ (kcal mol^{-1})	ΔH_{v4} (kcal mol^{-1})
N-NFU	100	134.6 ± 9.9	141.4 ± 4.2	**93.2 ± 9.8**	**79.2 ± 1.6**	-	-	-	-
	0	**59.1 ± 3.6**	**52.8 ± 1.4**	66.2 ± 3.4	70.1 ± 4.1	-	-	-	-
C-NFU	100	-	-	-	-	-	-	-	-
	0	-	-	-	-	-	-	-	-
N-NFU / C-NFU	100	42.0 ± 0.4	71.8 ± 5.8	**40.9 ± 0.4**	**60.4 ± 5.3**	**68.2 ± 1.5**	**71.9 ± 4.9**	289.4 ± 1.5	128.4 ± 38.4
	0	28.3 ± 1.2	48.9 ± 2.9	**38.2 ± 1.2**	**42.9 ± 3.4**	**28.2 ± 0.5**	**28.3 ± 2.6**	194.4 ± 0.6	105.6 ± 2.5
NFU	100	94.0 ± 7.1	41.8 ± 8.2	**20.1 ± 7.6**	**36.9 ± 3.3**	125.7 ± 7.9	69.0 ± 45.1	**37.9 ± 13.3**	**40.4 ± 2.7**
	0	**29.6 ± 9.3**	**32.9 ± 11.6**	57.3 ± 8.9	49.1 ± 29.9	**28.3 ± 4.9**	**32.2 ± 15.4**	102.8 ± 4.4	67.9 ± 1.9

By comparison with melting temperatures in Table 1, the enthalpic contribution from loss of secondary structure is listed in bold. In the cases of the N-NFU / C-NFU mixture and full-length NFU protein, two sets of enthalpies are observed due to the melting steps for the two independent domains.

Table 3

Circular dichroism analyses of N-terminal NFU, C-terminal NFU, a mixture of N- and C-terminal domains, and full-length NFU.

	N-NFU	C-NFU	N-NFU / C-NFU		NFU
			Experimental	Theoretical	
α-helix	31%	30%	32%	30 %	32%
β-sheet	21%	16%	18%	18%	20%
Random Coil	48%	54%	50%	52%	48%

Data were obtained at 25 °C with a path length of 0.1 cm and fit with the K2D3 program,[32] which yields a higher accuracy in β-strand prediction compared with its predecessor K2D.[13] Theoretical values for the N-NFU/C-NFU mixture were calculated from the average values of the two isolated domains.

Table 4

Melting temperatures of N-terminal NFU, C-terminal NFU, a mixture of N- and C- terminal domains, and full-length NFU determined by VTCD.

	[NaCl] (mM)	T_{m1} (°C)	T_{m2} (°C)
N-NFU	100.0	79.5 ± 0.4	
	0.0	75.7 ± 0.1	
C-NFU	100.0	59.4 ± 3.8	
	0.0	60.7 ± 0.5	
N-NFU / C-NFU	100.0	59.2 ± 0.5	78.6 ± 0.2
	0.0	41.9 ± 1.5	77.2 ± 0.3
NFU	100.0	67.8 ± 0.6	77.8 ± 0.9
	0.0	50.2 ± 1.2	71.0 ± 0.4

The melting points were determined from molar ellipticity data fit with equations 1 or 2. As a result of the broad transitions observed for the C-NFU domain, T_m's were estimated according to a single transition and indicated with asterisk marks. In rows containing data collected on a mixture of N-NFU / C-NFU and the full-length NFU, the T_{m1} and the T_{m2} parameters refer to melting temperatures for the C-terminal and N-terminal domains, respectively.

Table 5

Fitting parameters for the change in Van't Hoff enthalpy determined by VTCD.

	[NaCl] (mM)	ΔH_{v1} (kcal mol^{-1})	ΔH_{v2} (kcal mol^{-1})
N-NFU	100.0	69.6 ± 6.1	
	0.0	41.8 ± 4.5	
C-NFU	100.0	13.6 ± 3.2	
	0.0	17.7 ± 0.9	
N-NFU / C-NFU	100.0	43.3 ± 4.1	69.2 ± 1.1
	0.0	44.1 ± 4.5	45.8 ± 0.7
NFU	100.0	23.9 ± 1.7	41.0 ± 2.7
	0.0	31.8 ± 6.3	28.3 ± 3.3

Values were obtained from fitting the molar ellipticity versus temperature by use of equations 1 or 2. Increasing ionic strength resulted in an increase in the Van't Hoff enthalpy, indicating a relatively more stable secondary structure for well-folded domains, such as N-NFU, and consistent with the trends observed in the melting temperatures defined in Table 4.